In Vivo Imaging of Bone Using a Deep-Red Fluorescent Molecular Probe Bearing Multiple Iminodiacetate Groups

Kara M. Harmatys, Erin L. Cole, and Bradley D. Smith*

Department of Chemistry and Biochemistry, University of Notre Dame, 236 Nieuwland Science Hall, Notre Dame, 46556 Indiana, United States

Ⓢ Supporting Information

ABSTRACT: Deep-red fluorescent molecular probes are described that have a dendritic molecular architecture with a squaraine rotaxane core scaffold and multiple peripheral iminodiacetate groups as the bone targeting units. Iminodiacetates have an inherently lower bone affinity than bisphosphonates, and a major goal of the study was to determine how many appended iminodiacetate groups are required for effective deep-red fluorescence imaging of bone in living rodents. A series of in vitro and in vivo imaging studies showed that a tetra(iminodiacetate) probe stains bones much more strongly than an analogous bis(iminodiacetate) probe. In addition, a control tetra(iminodipropionate) probe exhibited no bone targeting ability. The tetra(iminodiacetate) probe targeted the same regions of high bone turnover as the near-infrared bisphosphonate probe OsteoSense750. Longitudinal studies showed that the fluorescence image signal from living mice treated with the tetra(iminodiacetate) probe was much more stable over 19 days than the signal from OsteoSense750. The narrow emission band of the tetra(iminodiacetate) probe makes it very attractive for inclusion in multiplex imaging protocols that employ a mixture of multiple fluorescent probes in preclinical studies of bone growth or in fluorescence guided surgery. The results also suggest that molecules or nanoparticles bearing multivalent iminodiacetate groups have promise as bone targeting agents with tunable properties for various pharmaceutical applications.

KEYWORDS: bone targeting, in vivo imaging, multivalency, iminodiacetate, fluorescence molecular imaging, squaraine rotaxane
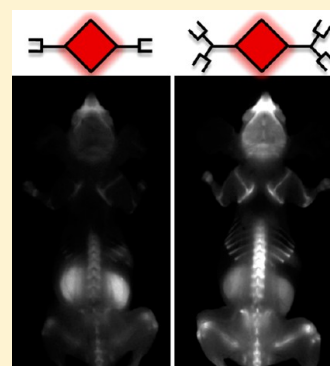
INTRODUCTION

The extracellular matrix of bone tissue has high mineral content and is especially rich in Ca^{2+} salts. A common feature of most bone-seeking agents is a strong affinity for metal cations.[1−3] For example, commercially available fluorescent dyes with Ca^{2+} chelation ability have been used for several decades to stain samples of bone and teeth.[4−9] Typically, the dyes emit visible wavelengths, which is a limitation for in vivo studies due to poor penetration of visible light through skin and tissue. It is well-recognized that biological imaging is improved by employing dyes that emit in the 650−900 nm window. Recently, several near-infrared bone probes have been reported, and in most cases the molecules are cyanine dyes with appended bisphosphonates as the bone targeting groups.[10−16] While bisphosphonates are known for their high affinity for bone surfaces undergoing structural turnover, their use as imaging agents has potential limitations. For example, bisphosphonates induce osteoclasts to undergo apoptosis; thus they can potentially disrupt the physiological process that they are supposed to be imaging.[17−19] Likewise, cyanine dyes are popular as near-infrared fluorophores, but they have some drawbacks, including moderate to poor long-term stability which limits their effectiveness in quantitative and longitudinal imaging studies.[20]

Here, we describe a new structural class of bone-seeking molecular probes with dendritic molecular structures. The central scaffold is a squaraine rotaxane, a new interlocked molecular architecture that encapsulates a highly fluorescent squaraine dye inside a surrounding protective macrocycle.[21] Squaraine rotaxanes are very well-suited for optical imaging as they exhibit intense and narrow absorption/emission bands with deep-red wavelengths. They are ideal for in vitro studies using microscopes and microarray systems equipped with standard Cy5 filter sets, and they also perform well as in vivo imaging agents with good penetration of the deep-red light through skin and tissue.[22−26] We have developed versatile synthetic chemistry methods that produce dendritic molecular structures with specific numbers of peripheral groups attached to a central squaraine rotaxane core.[27] In this report, we describe the preparation and evaluation of new squaraine rotaxane probes that are decorated with multiple iminodiacetate groups as the bone targeting units. Iminodiacetates have inherently lower bone affinity than bisphosphonates (Ca^{2+} association constants),[1] but we reasoned that probe association could be enhanced by creating multivalent versions. In addition to commercial visible dyes with two iminodiacetate groups, such as the green-emitting calcein, there are previous reports of
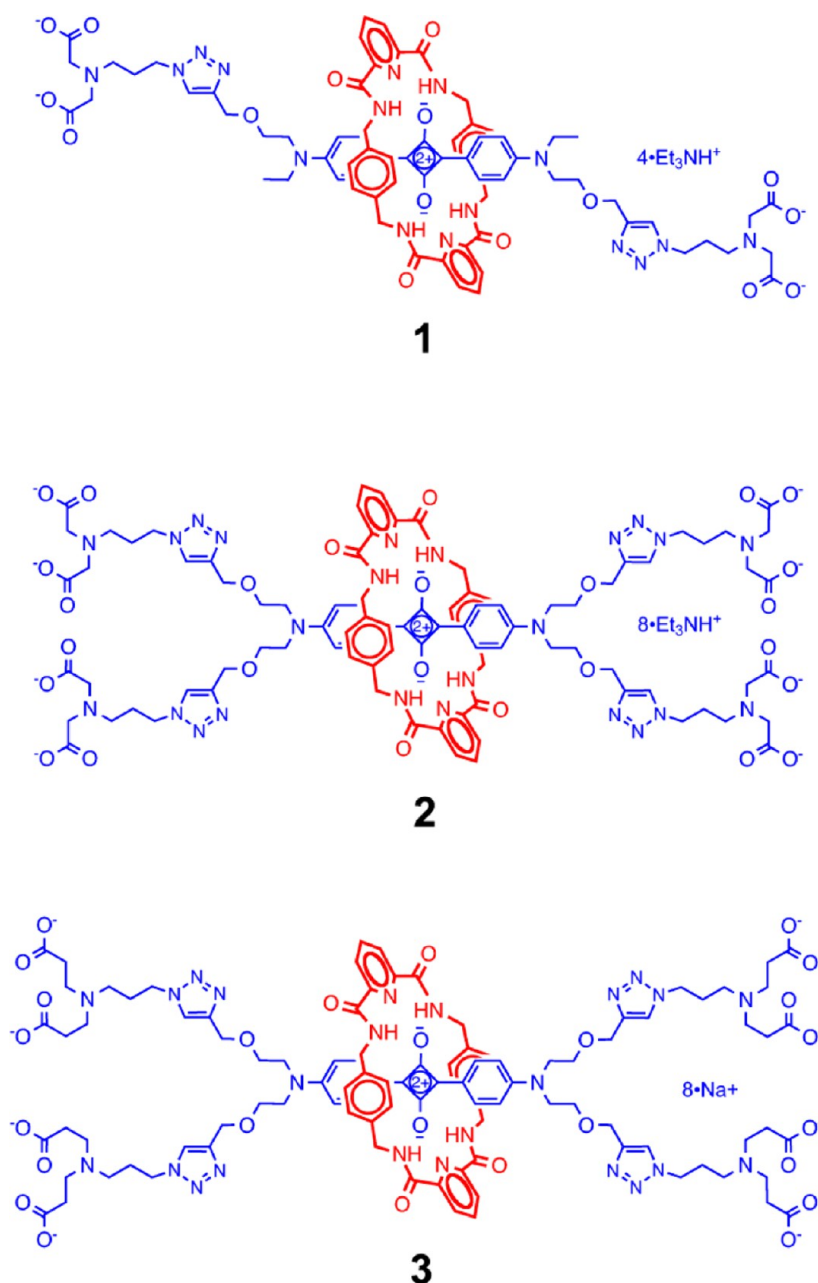
Figure 1. Structures of fluorescent squaraine rotaxane molecular probes; bis(iminodiacetate) **1**, tetra(iminodiacetate) **2**, and tetra-(iminodipropionate) **3**.

bone-seeking molecular probes with three or four iminodiacetate groups,[28,29] but none of these literature compounds were tested in vivo. Therefore, the primary goal of this study was to determine how many appended iminodiacetate groups are required for effective deep-red fluorescence imaging of bone in living animals. We report the results of in vitro and in vivo imaging studies that compare the bone targeting capabilities of the bis(iminodiacetate) **1** and the tetra(iminodiacetate) **2** (Figure 1). We also studied tetra(iminodipropionate) **3** as a structurally related, untargeted control probe that has negligible affinity for biological surfaces.[22,26] We find that tetra-(iminodiacetate) probe **2** is an effective deep-red fluorescent bone imaging agent and likely to be useful for various microscopic and live animal optical imaging studies. From a broader perspective, our results suggest that molecules or nanoparticle probes bearing multivalent iminodiacetate groups

have promise as bone targeting agents for various therapeutic and imaging applications.

■ MATERIALS AND METHODS

The probe syntheses are described in the Supporting Information, and the photophysical properties are listed in Table 1. OsteoSense750 was purchased from VisEn Medical (Bedford, MA) and Xylenol Orange from Sigma-Aldrich (Milwaukee, WI).

In Vitro Assay for Bone Binding. Tibia and femur bones were excised from Lobund Wistar rats and ground up to make bone powder. Targeted probe **2** or untargeted control probe **3** (4 μM) in water was combined with varying amounts of dried bone powder (0 to 200 mg) in separate centrifuge tubes and the tubes shaken for 1 h at room temperature. To separate the probe not bound to the bone powder, the tubes were

Table 1. Probe Photophysical Properties in Water

probe	λ_{abs} (nm)	$\log \varepsilon$	$\lambda_{em}{}^a$ (nm)	$\Phi_f{}^b$
1	655	5.00	675	0.10
2	653	5.15	677	0.13
3	653	5.20	674	0.23

^{a}Solutions were excited at optically matching wavelengths and emission monitored in the region 600−900 nm. ^{b}Fluorescence quantum yields (error limit ±5%) were determined using 4,4-[bis(N,N-dimethylamino)phenyl] squaraine dye as the standard (Φ_f = 0.70 in CHCl$_3$).

centrifuged at 1350g for 5 min, and the pellet of bone powder was discarded. A fluorescence spectrum (ex: 580 nm) of the unbound probe remaining in the supernatant was acquired, and fluorescence maxima intensities were normalized to the solution containing no bone powder.

In Vitro Bone Staining. All animal experiments used protocols that were approved by the Notre Dame Institutional Animal Care and Use Committee. The tibia and femur tissue from a SKH1 hairless mouse was excised and flash frozen in OCT media. Bone tissue was sliced (12 μm thickness) at −17 °C, and the slices adhered to Unifrost microscope slides (Azer Scientific, USA), then fixed with chilled acetone for 10 min, and air-dried for an additional 20 min. The tissue slices were submerged in either targeted probe **2** or untargeted control probe **3** (10 μM) in water for 1 h, then (a) washed with auto buffer in triplicate for 5 min intervals, (b) incubated with Image-IT FX Signal Enhancer (Invitrogen, Eugene, USA) for 15 min and washed three additional times, and (c) submerged in ProLong Gold Antifade Reagent (Invitrogen, Eugene, USA). Finally, a coverslip was adhered, and the slide was allowed to dry for at least 1 h. Bright field and deep-red fluorescence images of the slices were acquired using a Nikon TE-2000U epifluorescence microscope equipped with the appropriate Cy5 filter set (ex: 620/60, em: 700/75). Images were captured using NIS-Elements software (Nikon, USA) and analyzed using ImageJ 1.40g. The same protocol was used to costain bone tissue slices with the deep-red targeted probe **2** (observed using Cy5 filter set) and near-infrared OsteoSense750 (observed using Cy7 filter set, ex: 710/75, em: 810/90) with slices submerged sequentially in aqueous solutions of each probe for 30 min.

Multiprobe Imaging of Bone Layering in Rat. A 19-week old male Lobund Wistar rat was injected with Xylenol Orange (17 mg/kg) subcutaneously three days prior to administration of targeted probe **2** (1.9 mg/kg) via the tail vein. Twenty-four hours later, the rat was euthanized, and sections of femur and tibia were sliced at a thickness of 16 μm. The bone slices were processed and imaged as described in the bone staining section above, with the Xylenol Orange micrographs observed using a Cy3 filter set (ex: 535/50, em: 610/75 nm) and the probe micrographs observed using a Cy5 filter set.

In Vivo Mouse Imaging. Male SKH1 hairless mice were anesthetized (3% isoflurane inhalation) and given intraperitoneal injections of aqueous solutions of probe **1**, **2**, or **3** (20 nmol) in water. At appropriate time points, they were anesthetized and imaged using a Kodak In Vivo Multispectral Imaging Station FX (Carestream Health; Rochester, NY) configured for epi-illumination and planar X-ray imaging. The animals were illuminated with filtered deep-red light (630/10 nm), and an image of emission intensity at 700/20 nm was

collected using a charge-coupled device (CCD) camera and a 5 s acquisition period (bin = 2 × 2, f-stop = 2.51, field of view = 50 or 100 mm). The mice were imaged immediately after probe dosing and also at 1, 3, 6, and 24 h time points. The mice were euthanized via cervical dislocation immediately after the 24 h time point, and the skin was removed for further fluorescence imaging. A planar X-ray image was also acquired (120 s acquisition period, f-stop = 2.51, filter = 0.8 mm, field of view = 50 or 100 mm; bin = 0) of the skinless mice that had been injected with probe **2** (merged images in Figure 8). One set of experiments dosed a cohort of mice with two probes, intraperitoneal injection of targeted tetra(iminodiacetate) probe **2** (4 nmol) in water and retro-orbital injection of OsteoSense750 (2 nmol) in water (the two different routes of administration attenuate discomfort to the animal). Fluorescence images of probe **2** distribution were acquired using the filter set listed above (25 s time acquisition, bin 4 × 4, f-stop = 2.51, FOV = 50 mm or 100 mm), and OsteoSense750 distribution was imaged using a 730/10 nm excitation filter and 790/20 nm emission filter (30 s acquisition period, bin = 4 × 4, f-stop = b2.51, field of view = 50 or 100 mm).

Fluorescence Image Analysis. Animal images were analyzed using ImageJ 1.40g. The 16-bit images were imported, opened in sequential order, and converted to an image stack. Background subtraction was applied to the images using the rolling ball algorithm (radius = 500 pixels or 1000 pixels). The stack was then converted to a montage and pseudocolored as either "Grays" or "Red Hot" (under the "Lookup Tables" menu). Region of interest (ROI) analysis was performed by drawing a shape around the specific site and using the software to calculate mean pixel intensity. The ROI values were plotted using GraphPad Prism 5 (Graphpad Software Inc., San Diego, CA).

Cell Toxicity. Quantification of toxicity was measured using the 3-(4, 5-dimethylthiazol-2-yl)-2,5-diphenyltetrazolium bromide (MTT) cell viability assay. MDA-MB-231 human breast cancer cells (ATCC HTB-26) and Saos-2 human osteosarcoma cells (ATCC HTB-85) were purchased from American Type Culture Collection, seeded into 96-microwell plates, and grown to confluency of 85% in RPMI or McCoy's 5A media supplemented with 10% or 15% fetal bovine serum, and 1% streptavidin L-glutamate at 37 °C and 5% CO$_2$. The Vybrant MTT cell proliferation assay kit (Invitrogen, Eugene, USA) was performed according to the manufacturer's protocol and validated using 50 μM etoposide as a positive control for high toxicity. The cells were treated with bis(iminodiacetate) probe **1** and tetra(iminodiacetate) probe **2** (0−100 μM) and incubated for 18 h at 37 °C. The medium was removed and replaced with 100 μL of RPMI or McCoy's media containing [3-(4,5-dimethylthiazol-2-yl)-2,5-diphenyltetrazolium bromide] (MTT, 1.2 mM) and the sample incubated for 4 h at 37 °C and 5% CO$_2$. An SDS−HCl detergent solution was added and incubated for an additional 4 h. The absorbance of each well was measured at 570 nm ($N = 4$), and the data were normalized to untreated cells. Only active reductase enzymes in living cells can reduce MTT; therefore high levels of cell viability are indicated by high absorbance at 570 nm.

Histopathology. A cohort of SKH1 hairless mice ($N = 3$) were given an intraperitoneal injection of tetra(iminodiacetate) probe **2** (20 nmol) in water and euthanized 24 h later. Kidney, liver, spleen, and mineralized bone tissues were excised, fixed, then embedded and flash frozen in OCT. Tissue sections were

stained with haematoxylin/eosin and compared microscopically to tissues taken from a cohort of untreated mice ($N = 3$).

RESULTS

Fluorescent molecular probes **1**−**3** are highly water-soluble compounds that were prepared by conducting "clicked" cycloaddition reactions that attached the peripheral functional groups to a central squaraine rotaxane core (see Supporting Information). Squaraine rotaxanes are deep-red fluorophores with intense narrow absorption and emission bands, high chemical stability, and good quantum yields in aqueous solution. The photophysical properties for fluorescent probes **1**−**3** are listed in Table 1.

Initial experiments qualitatively compared the affinity of targeted tetra(iminodiacetate) probe **2** and untargeted control probe **3** for bone powder in aqueous solution. Separate solutions of **2** or **3** were treated with increasing amounts of bone powder and shaken for 1 h. The bone powder was removed by centrifugation, and the amount of probe remaining in the supernatant was determined by a fluorescence spectroscopy. The normalized spectra in Figure S3 show that 200 mg of bone powder removed >40% of targeted probe **2** from the solution, whereas there was no measurable extraction of untargeted control probe **3**. The lack of bone affinity exhibited by probe **3** is consistent with previous studies, showing that it has negligible affinity for biological surfaces.[22,26]

A separate set of microscopy experiments assessed the ability of the probes to stain thinly sliced sections of mouse bone tissue. The microscopy images in Figures 2 and 3 show bone
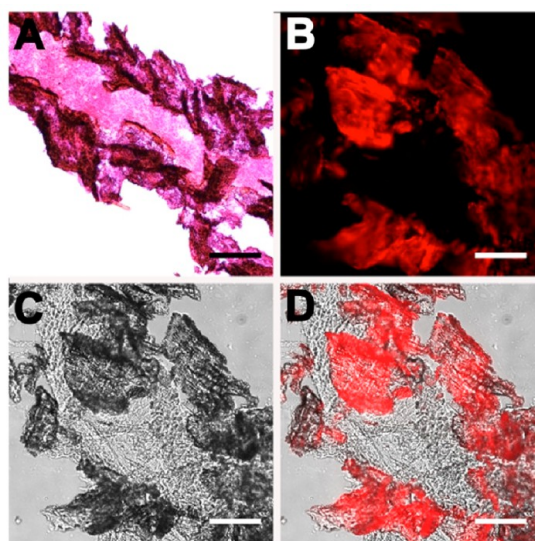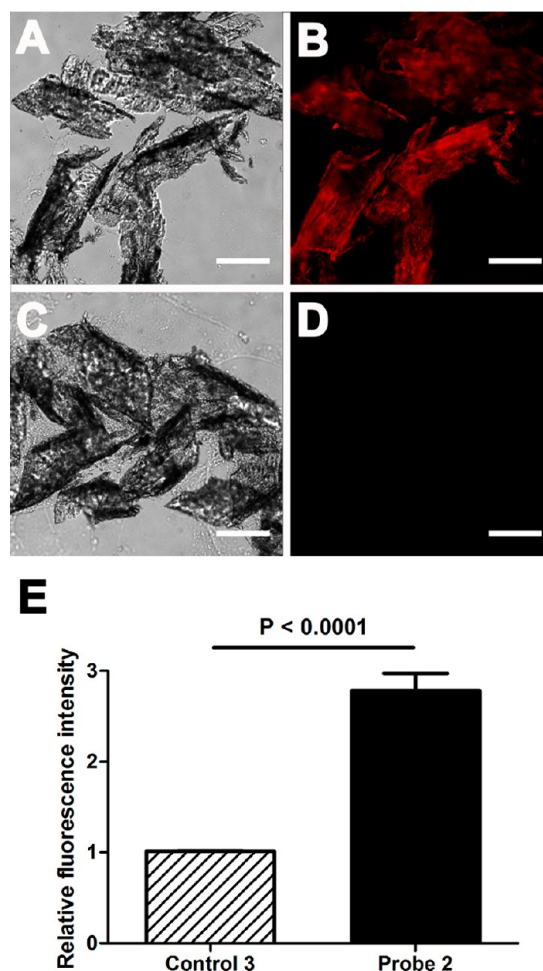

Figure 3. Representative histological slices of tibia extracted from a healthy SKH1 mouse. The slices were incubated with targeted probe 2 (10 μM) (A−B) or untargeted control 3 (10 μM) (C−D) in water for 1 h. Micrographs were acquired using brightfield (A, C) or Cy5 fluorescence (B, D) filter sets. Scale bar = 0.16 mm for all panels. The graph (E) shows the relative ratio of fluorescence mean pixel intensity for panels B and D and is normalized to the fluorescence of control 3 ($N = 5$).

Figure 2. Representative histological slices of tibia extracted from a healthy SKH1 mouse. The slices were subjected either to hematoxylin/eosin staining (A) or incubation with targeted probe **2** (10 μM) in water (B−D) for 1 h. The brightfield image (C) and deep-red fluorescence emission image due to staining by probe **2** (B) is merged in panel D. Scale bar = 0.16 mm for all panels.

slices after they were incubated with targeted probe **2** or untargeted control probe **3** for 1 h and washed with buffer. The deep-red fluorescence image in Figure 2D shows localization of **2** to calcified areas of the bone section. In comparison, there was much weaker bone staining by **3** (Figure 3). Evidence that targeted probe **2** was associating with the Ca^{2+} ions in the bone sections was gained by showing that the probe did not stain

bone slices that had been pretreated for 16 h with 0.25 M of the Ca^{2+}-chelating agent EDTA (Figure 4). The in vitro staining profile of probe **2** was assessed by costaining with the commercially available OsteoSense750, a fluorescent bisphosphonate imaging agent with near-infrared emission. Reasonably high colocalization of near-infrared OsteoSense750 and deep-red probe **2** was observed in the merged fluorescence bone micrographs (Figure S4) suggesting that both probe molecules were primarily targeting the same mineralized sites on the bone.

The promising in vitro bone staining results prompted us to conduct in vivo optical imaging studies that compared the bone targeting abilities of the different fluorescent probes. The first study compared targeted probe **2** and untargeted control probe **3** for ability to label the skeletons of living mice. Two separate cohorts of three mice were anesthetized and given an intraperitoneal injection of **2** or **3** (20 nmol) in water. Following probe dosing, the living animals were imaged periodically over 24 h using a planar, whole-body fluorescence imaging station with a deep-red filter set (ex: 630 nm, em: 700 nm). A comparison of the two sets of longitudinal images
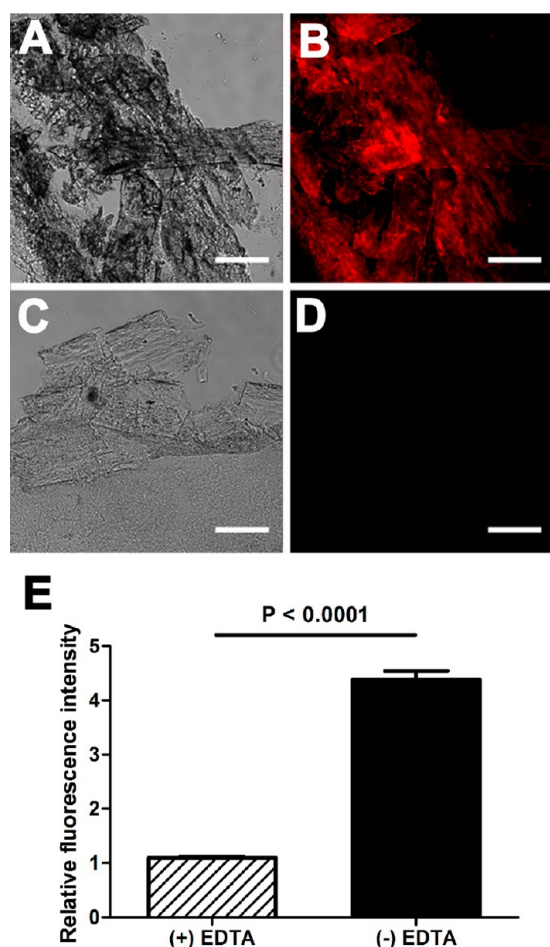
Figure 4. Representative histological slices of tibia extracted from a healthy SKH1 mouse. The slices were subjected to decalcification for 16 h with 0.25 M EDTA (C, D) or no incubation with EDTA (A, B), then subjected to incubation with targeted probe **2** (10 μM) in water for 1 h. Micrographs were acquired using the brightfield (A, C) or Cy5 fluorescence (B, D) filter sets. Scale bar = 0.16 mm for all panels. The graph (E) shows the relative ratio of fluorescence mean pixel intensity for panels B and D which is normalized to the fluorescence of cells treated with EDTA ($N = 5$).

(Figure S5) showed that the targeted probe **2** strongly stained the mouse skeleton, whereas untargeted control probe **3** exhibited no bone affinity. The next experiment compared the bone targeting abilities of divalent probe **1** and tetravalent probe **2** in living mice. Two cohorts of mice ($N = 3$) were treated with either probe (20 nmol). The in vivo images in Figure 5 (with corresponding quantitative analysis in Figure 6) show that the tetravalent probe **2** targeted the bones of living mice with a significantly higher affinity than probe **1**. An additional study showed that a 10-fold lower dose of probe **2** (2 nmol) still produced higher bone imaging contrast in living mice than 20 nmol of probe **1** (compare Figures 5 and S7). The images in Figures 7 and 8 include higher clarity, ex vivo fluorescence images of the skinless animals after euthanization at the 24 h time point. They indicate strong localization of probe **2** at skeletal regions that have high bone turnover, such as tibial and femoral heads, lumbar vertebrae, and scapulae.

The bone targeting preference was further assessed by conducting a multicolor imaging experiment that dosed a cohort of mice with deep-red probe **2** and also near-infrared OsteoSense750. Twenty four hours after dosing, the animals were euthanized, the skin removed, and fluorescence images taken using the appropriate filter sets. The multicolor images in Figure 9 show extensive colocalization of the two molecular probes at the same skeletal positions.

A notable characteristic of squaraine rotaxane dyes is their extremely high chemical stability, and this was highlighted by comparing the time-dependent decrease in bone signal in mice that had either been treated with a single dose of probe **2** or OsteoSense750. Shown in Figure S8 is the normalized change in mean pixel intensity over 19 days for a region of interest on the spine of mice. Quantitative analysis of the imaging data showed that fluorescence intensity for mice treated with OsteoSense750 decreased to about 50% of original value, whereas the fluorescence intensity for mice treated with probe **2** remained above 90% of original value.

A multicolor bone growth monitoring experiment was conducted using a combination of the green/orange emitting fluorescent dye, Xylenol Orange (known to target areas of bone turnover), and deep-red targeted probe **2**. A 19-week old male Lobund Wistar rat was injected with Xylenol Orange (17 mg/kg) at $t = 0$, followed by the targeted probe **2** (1.9 mg/kg) at $t = 4$ days. The rat was euthanized at $t = 5$ days, and sections of femur and tibia were sliced at a thickness of 16 μm. Shown in Figures 10 and S9 are representative multicolor fluorescent images of the bone sections. The images show two distinct layers of probe staining, with the layer stained by probe **2** closer to the exterior surface of the bone, an observation that is consistent with bone growth during the four day interval between probe dosages.

The results of two separate experiments indicate that probe **2** is not an acutely toxic molecule. First, standard MTT cell viability assays (Figures S10 and S11) showed that doses up to 100 μM of the different squaraine rotaxane probes had little effect on the viability of cultured MDA-MB-231 human breast cancer cells or Saos-2 human osteosarcoma cells. In addition, histopathological comparisons of bone and the clearance organs from untreated mice and mice treated with a single dose of probe **2** and euthanized 24 h later showed no evidence of probe toxicity (Figure S12).

■ DISCUSSION

The chemical syntheses of squaraine rotaxane probes **1**−**3** were achieved in good yield and high mass throughput. The compounds have intense and narrow absorption/emission bands with reasonable quantum yields for deep-red fluorophores in aqueous solution. The mouse imaging studies clearly indicate that the tetra(iminodiacetate) probe **2** binds the animal skeleton more strongly than bis(iminodiacetate) probe **1**. Probe **2** does not stain decalcified bone, which is strong evidence that the bone targeting is primarily due to the Ca^{2+} chelation ability of the four appended iminodiacetate groups. Further support for this binding model is the lack of bone targeting exhibited by the control probe **3** which has a very similar core chemical structure but contains four peripheral iminodipropionate groups that have very weak affinity for Ca^{2+}.[30]

In a living mouse, about half of an intravenous dose of probe **2** reaches the bones with the rest being cleared rapidly through the kidneys (Figures 5 and 6). High renal clearance is a characteristic of molecules and small nanoparticles (i.e., diameter ≤5.5 nm) that have a mixed and geometrically balanced distribution of positive and negative charges.[31] The dendritic and polyionic structure of probe **2** (primarily a mixture of eight anionic carboxylates and four cationic
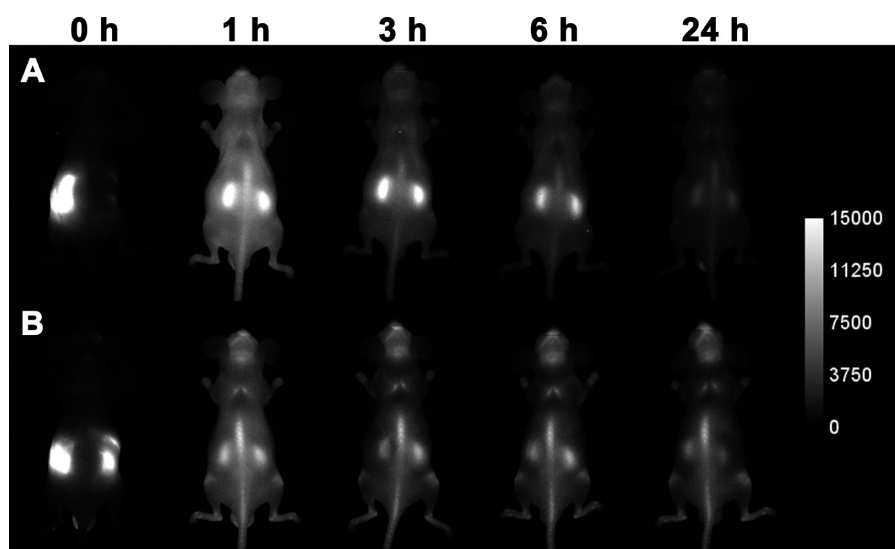
Figure 5. Representative deep-red fluorescent dorsal images of living mice treated with 20 nmol of divalent probe 1 (A) or tetravalent probe 2 (B). Images were acquired at the indicated time points after intraperitoneal injection the molecular probe in water ($N = 3$). The fluorescence pixel intensity scale bar applies to all images. Lateral images of the same animals are shown in Figure S6.
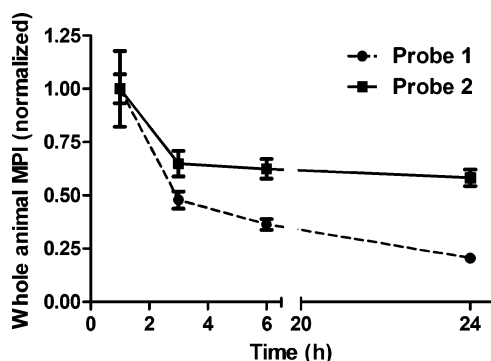

Figure 6. ROI analysis of the mouse imaging data in Figure 5. The graph shows mean pixel intensity, normalized to the 1 h postinjection time point, for the whole animal treated with 20 nmol of divalent probe 1 (dotted line) or tetravalent probe 2 (solid line). Error bars represent the standard error mean ($N = 3$).
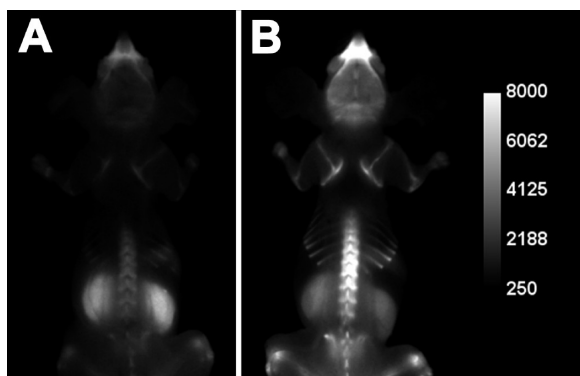

Figure 7. Representative deep-red fluorescent dorsal image of two skinless mice that had been dosed with 20 nmol of divalent probe 1 (A) or tetravalent probe 2 (B) and euthanized 24 h later. The fluorescence pixel intensity scale bar applies to both images ($N = 3$).
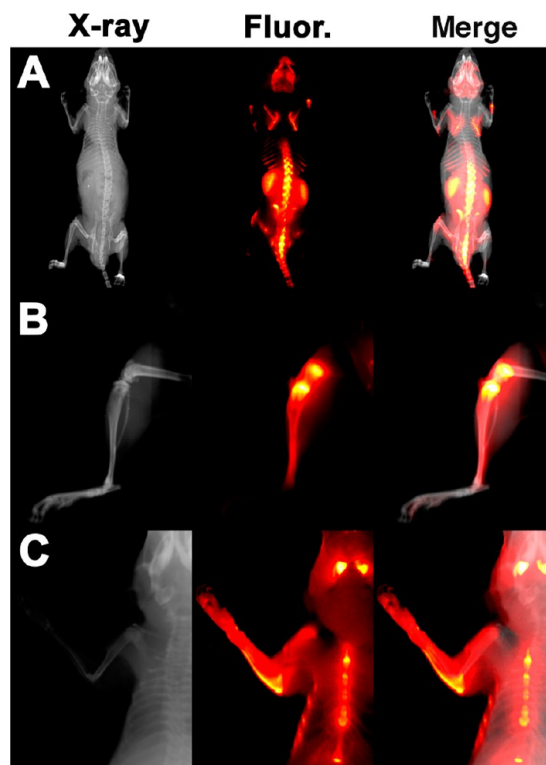

Figure 8. Representative dorsal (A), leg (B), and chest (C) images of a skinless mouse. The X-ray, deep-red fluorescence, and merged images show a SKH1 hairless mouse that had been dosed with 20 nmol of probe **2** and euthanized 24 h later ($N = 3$).

ammoniums at physiological pH) favors extensive hydration of the molecular periphery and avoidance of biological surfaces,

while maintaining moderate affinity for the mineralized components of bone.

The multicolor mouse images in Figure 9 show that probe **2** and the bisphosphonate probe OsteoSense750 both target the same skeletal regions that are undergoing relatively high amounts of bone turnover.[11−14] Longitudinal monitoring of the skeleton fluorescence intensity over 19 days (a time period that is sometimes required for bone growth studies) showed a large
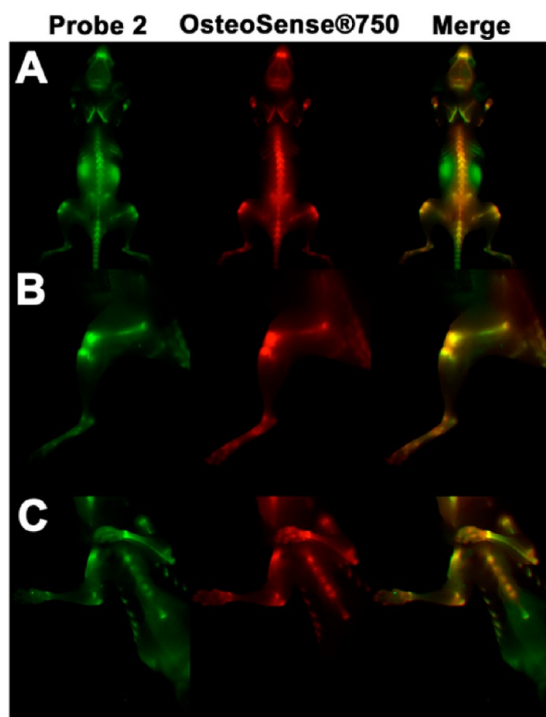
Figure 9. Representative dorsal (A), leg (B), and chest (C) in vivo fluorescence images of skinless mice that had been treated with probe **2** (4 nmol) via an intraperitoneal injection and OsteoSense750 (2 nmol) via an retro-orbital injection. The images were acquired immediately after euthanization at 24 h postinjection of the probes and show fluorescence from probe **2** (ex: 630/10 nm, em: 700/20 nm), fluorescence from OsteoSense750 (ex: 730/10 nm, em: 790/20 nm), and a merged image ($N = 3$).
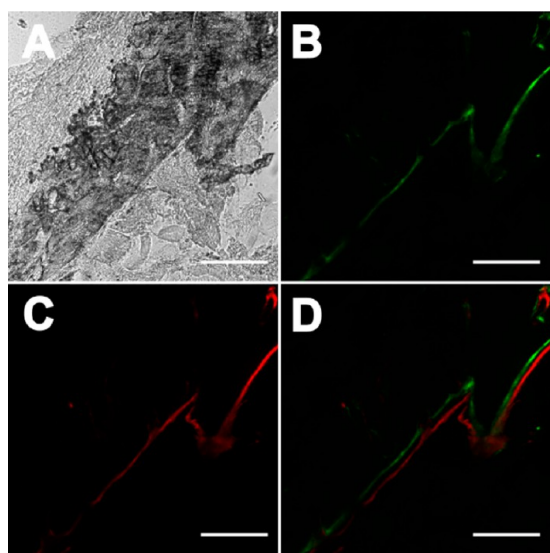

Figure 10. Representative histological slice from the tibia of a healthy young rat injected at $t = 0$ with Xylenol Orange (17 mg/kg), then probe **2** (1.9 mg/kg) at $t = 4$ days, and euthanized at $t = 5$ days. A: brightfield image; B: fluorescence image showing Xylenol Orange (ex: 535 nm, em: 610 nm); C: fluorescence image showing probe **2** (ex: 630 nm, em: 700 nm); D: merge of panels B and C. Scale bar = 0.16 mm.

signal decrease in the living mice treated with OsteoSense750 and only a small signal decrease with the mice treated with probe **2** (Figure S8). This difference is attributed to the higher

chemical stability of probe **2** and suggests that it may be quite useful for quantitative long-term imaging studies of bone growth. The narrow emission band of probe **2** makes it very attractive for inclusion in multiplex imaging protocols that employ multiple fluorescent probes. Two types of molecular imaging applications can be envisioned. One application sequentially treats animal models with a series of differently colored fluorescent bone-seeking probes and measures the amount of new bone growth between the colored layers in microscopic bone sections that are prepared ex vivo at the end of the experiment.[4−9] A range of commercially available visible probes are already known, and probe **2** adds a versatile deep-red wavelength channel to the portfolio. A second potential application with deep-red probe **2** is fluorescence guided surgery, a rapidly advancing technology that is enhanced by the use of deep-red and near-infrared fluorescent probes.[32] An emerging paradigm employs a real-time fluorescence imaging platform with two emission channels (deep-red and near-infrared) to identify targeted probe localization at two complementary sites in a surgical field (e.g., bone tissue, cancer cells, lymph nodes, nerves). The deep-red emission wavelength for probe **2** is well-suited as one of these two observation channels for identifying areas of viable bone that are still undergoing turnover.[33]

From a broader perspective beyond molecular imaging, bone-seeking agents have potential value as targeting groups for pharmaceutical applications such as drug delivery,[34] bone repair,[35] or osteogenic differentiation.[36] The targeting group can be directly attached to the pharmaceutical agent to form a monomeric or polymer conjugate;[37−41] or alternatively, the surface of an appropriate nanocapsule delivery vehicle can be coated with multiple copies of a targeting group.[42−44] Our results suggest that multivalent molecules or nanoparticles bearing iminodiacetate groups have promise as bone-seeking agents with tunable in vivo affinities and pharmacokinetic properties for a range of therapeutic and imaging applications.

■ ASSOCIATED CONTENT

Ⓢ Supporting Information
Synthetic procedures and structural characterization, additional in vitro bone staining and animal images, cell toxicity, and histopathology. This material is available free of charge via the Internet at http://pubs.acs.org.

■ AUTHOR INFORMATION

Corresponding Author
*E-mail: smith.115@nd.edu.

Notes
The authors declare no competing financial interest.

■ ACKNOWLEDGMENTS

■ REFERENCES

(1) Kubicek, V.; Lukes, I. Bone-seeking probes for optical and magnetic resonance imaging. *Future Med. Chem.* **2010**, *2*, 521−531.

(2) Low, S. A.; Kopeček, J. Targeting polymer therapeutics to bone. *Adv. Drug Delivery Rev.* **2012**, *64*, 1189−1204.

(3) Wang, D.; Miller, S. C.; Shlyakhtenko, L. S.; Portillo, A. M.; Liu, X.-M.; Papangkorn, K.; Kopečková, P.; Lyubchenko, Y.; Higuchi, W. I.;

Kopeček, J. Osteotropic peptide that differentiates functional domains of the skeleton. *Bioconjugate Chem.* **2007**, *18*, 1375−1378.

(4) Pautke, C.; Vogt, S.; Tischer, T.; Wexel, G.; Deppe, H.; Milz, S.; Schieker, M.; Kolk, A. Polychrome labeling of bone with seven different fluorochromes: enhancing fluorochrome discrimination by spectral image analysis. *Bone* **2005**, *37*, 441−445.

(5) Stuart, A. J.; Smith, D. A. Use of the fluorochromes xylenol orange, calcein green, and tetracycline to document bone deposition and remodeling in healing fractures in chickens. *Avian Dis.* **1992**, *36*, 447−449.

(6) van Gaalen, S. M.; Kruyt, M. C.; Geuze, R. E.; de Bruijn, J. D.; Alblas, J.; Dhert, W. J. A. Use of fluorochrome labels in in vivo bone tissue engineering research. *Tissue Eng., Part B* **2010**, *16*, 209−217.

(7) Pautke, C.; Tischer, T.; Vogt, S.; Haczek, C.; Deppe, H.; Neff, A.; Horch, H.-H.; Schieker, M.; Kolk, A. New advances in fluorochrome sequential labelling of teeth using seven different fluorochromes and spectral image analysis. *J. Anat.* **2007**, *210*, 117−121.

(8) Pautke, C.; Vogt, S.; Kreutzer, K.; Haczek, C.; Wexel, G.; Kolk, A.; Imhoff, A. B.; Zitzelsberger, H.; Milz, S.; Tischer, T. Characterization of eight different tetracyclines: advances in fluorescence bone labeling. *J. Anat.* **2010**, *217*, 76−82.

(9) Kovar, J. L.; Xu, X.; Draney, D.; Cupp, A.; Simpson, M. A.; Olive, D. M. Near-infrared-labeled tetracycline derivative is an effective marker of bone deposition in mice. *Anal. Biochem.* **2011**, *416*, 167−173.

(10) Bhushan, K. R.; Misra, P.; Liu, F.; Mathur, S.; Lenkinski, R. E.; Frangioni, J. V. Detection of breast cancer microcalcifications using a dual-modality SPECT/NIR fluorescent probe. *J. Am. Chem. Soc.* **2008**, *130*, 17648−17649.

(11) Wen, D.; Qing, L.; Harrison, G.; Golub, E.; Akintoye, S. O. Anatomic site variability in rat skeletal uptake and desorption of fluorescently labeled bisphosphonate. *Oral Dis.* **2011**, *17*, 427−432.

(12) Zaheer, A.; Lenkinski, R. E.; Mahmood, A.; Jones, A. G.; Cantley, L. C.; Frangioni, J. V. In vivo near-infrared fluorescence imaging of osteoblastic activity. *Nat. Biotechnol.* **2001**, *19*, 1148−1154.

(13) Kozloff, K. M.; Volakis, L. I.; Marini, J. C.; Caird, M. S. Near-infrared fluorescent probe traces bisphosphonate delivery and retention in vivo. *J. Bone Miner. Res.* **2010**, *25*, 1748−1758.

(14) Kozloff, K. M.; Weissleder, R.; Mahmood, U. Noninvasive optical detection of bone mineral. *J. Bone Miner. Res.* **2007**, *22*, 1208−1216.

(15) Kozloff, K. M.; Quinti, L.; Patntirapong, S.; Hauschka, P. V.; Tung, C.-H.; Weissleder, R.; Mahmood, U. Non-invasive optical detection of cathepsin K-mediated fluorescence reveals osteoclast activity in vitro and in vivo. *Bone* **2009**, *44*, 190−198.

(16) Bhushan, K. R.; Tanaka, E.; Frangioni, J. V. Synthesis of conjugatable bisphosphonates for molecular imaging of large animals. *Angew. Chem., Int. Ed.* **2007**, *46*, 7969−7971.

(17) Stern, P. H. Antiresorptive agents and osteoclast apoptosis. *J. Cell. Biochem.* **2007**, *101*, 1087−1096.

(18) Baron, R.; Ferrari, S.; Russell, R. G. G. Denosumab and bisphosphonates: different mechanisms of action and effects. *Bone* **2011**, *48*, 677−92.

(19) Russell, R. G. G. Bisphosphonates: the first 40 years. *Bone* **2011**, *49*, 2−19.

(20) Kassab, K. Photophysical and photosensitizing properties of selected cyanines. *J. Photochem. Photobiol., B* **2002**, *68*, 15−22.

(21) Gassensmith, J. J.; Baumes, J. M.; Smith, B. D. Discovery and early development of squaraine rotaxanes. *Chem. Commun.* **2009**, 6329−6338.

(22) Smith, B. A.; Xie, B. W.; van Beek, E. R.; Que, I.; Blankevoort, V.; Xiao, S.; Cole, E. L.; Hoehn, M.; Kaijzel, E. L.; Lowik, C. W.; Smith, B. D. Multicolor fluorescence imaging of traumatic brain injury in a cryolesion mouse model. *ACS Chem. Neurosci.* **2012**, *3*, 530−537.

(23) White, A. G.; Fu, N.; Leevy, W. M.; Lee, J. J.; Blasco, M. A.; Smith, B. D. Optical imaging of bacterial infection in living mice using deep-red fluorescent squaraine rotaxane probes. *Bioconjugate Chem.* **2010**, *21*, 1297−12304.

(24) Gassensmith, J. J.; Arunkumar, E.; Barr, L.; Baumes, J. M.; DiVittorio, K. M.; Johnson, J. R.; Noll, B. C.; Smith, B. D. Self-assembly of fluorescent inclusion complexes in competitive media including the interior of living cells. *J. Am. Chem. Soc.* **2007**, *129*, 15054−15059.

(25) Johnson, J. R.; Fu, N.; Arunkumar, E.; Leevy, W. M.; Gammon, S. T.; Piwnica-Worms, D.; Smith, B. D. Squaraine rotaxanes: superior substitutes for cy-5 in molecular probes for near-infrared fluorescence cell imaging. *Angew. Chem., Int. Ed.* **2007**, *46*, 5528−5231.

(26) Cole, E. L.; Arunkumar, E.; Xiao, S.; Smith, B. A.; Smith, B. D. Water-soluble, deep-red fluorescent squaraine rotaxanes. *Org. Biomol. Chem.* **2012**, *10*, 5769−5773.

(27) Xiao, S.; Fu, N.; Peckham, K.; Smith, B. D. Efficient synthesis of fluorescent squaraine rotaxane dendrimers. *Org. Lett.* **2010**, *12*, 140−143.

(28) Parkesh, R.; Gowin, W.; Lee, T. C.; Gunnlaugsson, T. Synthesis and evaluation of potential CT (computer tomography) contrast agents for bone structure and microdamage analysis. *Org. Biomol. Chem.* **2006**, *4*, 3611−3617.

(29) McMahon, B.; Mauer, P.; Mccoy, C. P.; Lee, T. C.; Gunnlaugsson, T. Selective imaging of damaged bone structure (microcracks) using a targeting supramolecular Eu(III) complex as a lanthanide luminescent contrast agent. *J. Am. Chem. Soc.* **2009**, *131*, 17542−17543.

(30) Chaberek, S.; Martell, A. E. Stability of Metal Chelates. I. Iminodiacetic and iminodipropionic acids. *J. Am. Chem. Soc.* **1952**, *74*, 5052−5056.

(31) Choi, H. S.; Nasr, K.; Alyabyev, S.; Feith, D.; Lee, J. H.; Kim, S. H.; Ashitate, Y.; Hyun, H.; Patonay, G.; Strekowski, L.; Henary, M.; Frangioni, J. V. Synthesis and in vivo fate of zwitterionic near-infrared fluorophores. *Angew. Chem., Int. Ed.* **2011**, *50*, 6258−6263.

(32) Keereweer, S.; Kerrebijn, J. F.; Driel, P. A. A.; Xie, B.; Kaijzel, E.; Snoeks, T. A.; Que, I.; Hutteman, M.; Vorst, J.; Mieog, J. S.; Vahrmeijer, A.; Velde, C. H.; Baatenburg de Jong, R.; Löwik, C. G. M. Optical image-guided surgery—where do we stand? *Mol. Imag. Biol.* **2011**, *13*, 199−207.

(33) Pautke, C.; Bauer, F.; Tischer, T.; Kreutzer, K.; Weitz, J.; Kesting, M.; Hölzle, F.; Kolk, A.; Stürzenbaum, S. R.; Wolff, K.-D. Fluorescence-guided bone resection in bisphosphonate-associated osteonecrosis of the jaws. *J. Oral Maxil. Surg.* **2009**, *67*, 471−476.

(34) Wang, D.; Miller, S.; Sima, M.; Kopečková, P.; Kopeček, J. Synthesis and evaluation of water-soluble polymeric bone-targeted drug delivery systems. *Bioconjugate Chem.* **2003**, *14*, 853−859.

(35) Brounts, S. H.; Lee, J. S.; Weinberg, S.; Lan Levengood, S. K.; Smith, E. L.; Murphy, W. L. High affinity binding of an engineered, modular peptide to bone tissue. *Mol. Pharmacol.* **2013**, *10*, 2086−2090.

(36) Lee, J. S.; Lee, J. S.; Murphy, W. L. Modular peptides promote human mesenchymal stem cell differentiation on biomaterial surfaces. *Acta Biomater.* **2010**, *6*, 21−28.

(37) Clementi, C.; Miller, K.; Mero, A.; Satchi-Fainaro, R.; Pasut, G. Dendritic poly(ethylene glycol) bearing paclitaxel and alendronate for targeting bone neoplasms. *Mol. Pharmaceutics* **2011**, *8*, 1063−1072.

(38) Hochdörffer, K.; Abu Ajaj, K.; Schäfer-Obodozie, C.; Kratz, F. Development of novel bisphosphonate prodrugs of doxorubicin for targeting bone metastases that are cleaved pH dependently or by cathepsin B: synthesis, cleavage properties, and binding properties to hydroxyapatite as well as bone matrix. *J. Med. Chem.* **2012**, *55*, 7502−7515.

(39) Yewle, J. N.; Puleo, D. A.; Bachas, L. G. Enhanced affinity bifunctional bisphosphonates for targeted delivery of therapeutic agents to bone. *Bioconjugate Chem.* **2011**, *22*, 2496−2506.

(40) Doschak, M. R.; Kucharski, C. M.; Wright, J. E. I.; Zernicke, R. F.; Uludağ, H. Improved bone delivery of osteoprotegerin by bisphosphonate conjugation in a rat model of osteoarthritis. *Mol. Pharmaceutics* **2009**, *6*, 634−640.

(41) Hrubý, M.; Etrych, T.; Kučka, J.; Forsterová, M.; Ulbrich, K. Hydroxybisphosphonate-containing polymeric drug-delivery systems designed for targeting into bone tissue. *J. Appl. Polym. Sci.* **2006**, *101*, 3192−3201.

(42) Zhang, G.; Guo, B. S.; Wu, H.; Tang, T.; Zhang, B. T.; Zheng, L. Z.; He, Y. X.; Yang, Z. J.; Pan, X. H.; Chow, H.; To, K.; Li, Y. P.; Li, D. H.; Wang, X. L.; Wang, Y. X.; Lee, K.; Hou, Z. B.; Dong, N.; Li, G.; Leung, K.; Hung, L.; He, F. C.; Zhang, L. Q.; Qin, L. A delivery system targeting bone formation surfaces to facilitate RNAi-based anabolic therapy. *Nat. Med.* **2012**, *18*, 307−314.

(43) Wang, G.; Babadagğli, M. E.; Uludağ, H. Bisphosphonate-derivatized liposomes to control drug release from collagen/hydroxyapatite scaffolds. *Mol. Pharmaceutics* **2011**, *8*, 1025−1034.

(44) Liu, D.; Kramer, S. A.; Huxford-Phillips, R. C.; Wang, S.; Della Rocca, J.; Lin, W. Coercing bisphosphonates to kill cancer cells with nanoscale coordination polymers. *Chem. Commun.* **2012**, *48*, 2668−2670.